

Thermal Boundary Conductance and Phonon Transmission in Hexagonal Boron Nitride/Graphene Heterostructures

David B. Brown, Thomas L. Bougher, Xiang Zhang, Pulickel M. Ajayan, Baratunde A. Cola, and Satish Kumar*

Two-dimensional (2D) materials such as graphene and hexagonal boron nitride (h-BN) have attracted interest as a conductor/insulator pair in next-generation devices because of their unique physical properties; however, the thermal transport at the interfaces must be understood to accurately predict the performance of heterostructures composed of these materials. Time-domain thermoreflectance (TDTR) is used to estimate the thermal boundary conductance (TBC) at the interface of h-BN and graphene to be $34.5 (+11.6/-7.4) \text{ MW m}^{-2} \text{ K}^{-1}$. The advantage of TDTR is that it does not need to create a large temperature gradient at the interface of heterostructures, but it has not yet been used for h-BN/graphene interface. Phonon transmission and TBC at the h-BN/graphene interface are predicted by two different formulations of the diffuse mismatch model (DMM) for anisotropic materials. The analysis of phonon transmission and temperature dependence of TBC establishes the flexural branch in the *ab*-plane, and the *c*-plane longitudinal acoustic branch of graphene and h-BN are the dominant contributors when implementing both the DMM models. The methodology developed herein can be used to analyze heterostructures of other 2D materials.

1. Introduction

The isolation of stable, 2D crystals^[1] began a revolution in condensed matter physics and materials science. Graphene, a 2D material made up of a single layer up to a few layers of sp^2 -bonded carbon atoms, has attracted considerable interest because of its high intrinsic carrier mobility, mechanical strength, thermal conductivity, and optical transparency.^[2–6] Graphene can be stacked with other 2D materials such as insulating hexagonal boron nitride (h-BN) or transition metal dichalcogenides (TMDs) like molybdenum disulfide (MoS_2) or tungsten disulfide (WS_2) to build layered, van der Waals heterostructures.^[7–13] These hybrid heterostructures introduce compositional and structural diversities to further enrich the properties and applications of 2D materials.^[14–16] For example, h-BN can be used as a promising substrate for graphene-based field-effect transistors (FETs) and improve the

mobility of FETs' channels^[7,8,10] compared with SiO_2 . In addition, graphene/h-BN and graphene/TMD heterostructures showed improved ON-OFF ratio in FET operation due to quantum tunneling.^[9,12] The thermoelectric properties of graphene/h-BN heterostructures have also been investigated.^[17,18] In-plane graphene/h-BN heterostructures possessing unique qualities which differ from the isolated parent materials are also a subject of active research.^[19–25]


Different stacking arrangements in graphene/h-BN vertical heterostructures are possible, resulting in different electronic and phononic properties.^[26–31] Heat dissipation from atomically thin 2D layers is limited by interfacial transport^[32] and makes them an ideal material system for the study of interfacial thermal transport. A fundamental understanding of phonon transport and estimation of the thermal boundary conductance (TBC), also known as Kapitza conductance,^[33] at the interfaces in 2D material heterostructures is critical to the design process to improving heat dissipation from these devices. Nevertheless, thermal transport across the interfaces in van der Waals heterostructures is still not well understood but is required to keep the device temperature below threshold and enable energy-efficient operation. Also, interface quality can vary from sample to sample and across samples based on preparation method, making it difficult to obtain an intrinsic measurement. Ultimately, proper control and characterization of the thermal interfaces in layered heterostructures are crucial for practical device applications.

The TBC at graphene/h-BN interfaces has been reported recently.^[31,34–38] Using first-principles atomistic Green's function (AGF) simulations, Mao et al.^[34] reported a room temperature (RT) TBC of $187 \text{ MW m}^{-2} \text{ K}^{-1}$ for a multilayer graphene/multilayer h-BN structure. Zhang et al.^[36] estimated

Dr. D. B. Brown, Dr. T. L. Bougher, Prof. B. A. Cola, Prof. S. Kumar
G. W. Woodruff School of Mechanical Engineering
Georgia Institute of Technology
Atlanta, GA 30332, USA
E-mail: satish.kumar@me.gatech.edu

Dr. X. Zhang, Prof. P. M. Ajayan
Department of Materials Science and NanoEngineering
Rice University
Houston, TX 77005, USA

Prof. B. A. Cola
School of Materials Science and Engineering
Georgia Institute of Technology
Atlanta, GA 30332, USA

 The ORCID identification number(s) for the author(s) of this article can be found under <https://doi.org/10.1002/pssa.201900446>.

DOI: 10.1002/pssa.201900446

the TBC at graphene nanoribbon/h-BN bilayer structure to be $5 \text{ MW m}^{-2} \text{ K}^{-1}$ at RT using classical molecular dynamics (MD) simulations. Yan et al.^[31] used first-principles simulations to study the effect of stacking arrangement on TBC for monolayer graphene sandwiched between layers of h-BN. The RT TBC values reported in this study ranged from 30 to $50 \text{ MW m}^{-2} \text{ K}^{-1}$. The first experimental measurement was performed by Chen et al.^[35] using Raman spectroscopy. The reported value of $7.4 \text{ MW m}^{-2} \text{ K}^{-1}$ was less than most of the theoretical calculations, which the authors attributed to trapped impurities resulting from the transfer process. Recently, Liu et al.^[37] measured TBC at graphene/h-BN to be $52.2 \text{ MW m}^{-2} \text{ K}^{-1}$ using the same Raman technique, whereas Kim et al.^[38] predicted TBC of $5\text{--}10 \text{ MW m}^{-2} \text{ K}^{-1}$ in electrically biased graphene FET on h-BN substrate.

Variation in TBC values calculated using different atomistic simulation techniques such as AGF and MD may be expected due to different assumptions and limitations. However, there is discrepancy in results even when the same measurement technique, Raman spectroscopy, is used. Also, the Raman technique requires a patterning step to form leads to electrically heating the graphene to create a temperature difference. In this work, time-domain thermoreflectance (TDTR), which requires only the deposition of a thin metal film, is used “for the first time” to estimate the TBC at the interfaces of graphene and h-BN. Our measured value of $34.5 \text{ MW m}^{-2} \text{ K}^{-1}$ lies in between the previously reported experimental values and also in the range of TBC predicted by first-principles density functional theory and AGF-based calculations.^[31] We also present phonon transmission and TBC predicted by two formulations of the diffuse mismatch model (DMM) for anisotropic materials like graphene and h-BN.

2. Experimental Section

Single-layer graphene (SLG), with some bilayer islands, and few-layer h-BN grown on Cu foil using separate chemical vapor deposition (CVD) processes^[39] were transferred to the surface of 300 nm thermally grown SiO₂ (measured using a Nanometrics Nanospec 3000 reflectometer) using a poly(methyl methacrylate) (PMMA) polymer support. Prior to transfer to SiO₂, the underlying Cu foil was etched in FeCl₃, and, following transfer, the PMMA was dissolved in acetone and isopropyl alcohol. A schematic of the transfer process is shown in the Supporting Information. Finally, the samples were annealed at 300 °C in vacuum (5–10 mTorr) to remove residual PMMA^[40] and improve conformity to the substrate.^[41] Raman spectroscopy data were acquired using a Renishaw InVia Raman microscope with 180° backscattering geometry and 488 nm Ar⁺ laser, focused using a 50× objective lens (NA = 0.5). X-ray photoelectron spectroscopy (XPS) was performed using a Thermo Scientific K-Alpha⁺ spectrometer with an Al K α monochromatic X-ray source (1486.6 eV). In preparation for thermal measurements, the samples were simultaneously coated with Au (3 nm Ti adhesion layer) using electron-beam evaporation to serve as thermal transducers. Schmidt et al.^[42] showed that inclusion of 5 nm Ti adhesion layer nearly doubled the TBC at the Al–graphite interface. Therefore, the interfaces considered here were Ti/G/SiO₂

or Ti/h-BN/SiO₂ despite a Au layer as the thermal transducer. The sample geometries used in this study are shown in **Figure 1a–c**. The actual film thickness of 77 nm (Figure 1) was measured on a codeposited glass slide using a Veeco Dimension 3100 Atomic Force Microscope in tapping mode.

TDTR has become a widely used technique to measure the thermal conductivity of thin films and substrates as well as TBC.^[43–47] Briefly, TDTR is a pump–probe optical technique, which uses a modulated laser beam (pump) to heat the surface of a sample and an unmodulated beam (probe) to measure the change in optical reflectivity of the surface. Modulation of the pump beam allows the signal to be measured using lock-in amplification. The experimental data were fit to a thermal model^[48] to extract the thermal properties of interest. In the two-color TDTR setup used in this study, described previously,^[49,50] the output of a Spectra Physics Ti:Sapphire ($\lambda = 800 \text{ nm}$, 40 nJ pulse^{-1}) laser with $\approx 150 \text{ fs}$ pulse width and a repetition rate of $\approx 80 \text{ MHz}$ was split into two beam paths (pump and probe) where the pump beam was modulated at a frequency of 8.8 MHz, then frequency doubled using a BiBO crystal. The pump and probe struck the surface concentrically at a normal angle of incidence and were focused to $1/e^2$ radii of ≈ 5 and $\approx 3 \mu\text{m}$, respectively, using pump and probe powers of 10 and 4 mW, respectively. The arrival time of the probe was delayed up to 5 ns relative to the pump by adjusting its optical length using a double-pass mechanical delay stage to map the decay of the thermoreflectance signal. Monte Carlo (MC) simulations were used to determine uncertainties associated with TBC estimation.

Crude models, such as the acoustic mismatch model (AMM),^[51–53] DMM,^[54–58] and similar variations like the maximum transmission limit (MTL)^[59,60] and radiation limit (RL),^[61–63] are popular for calculation of TBC. The main difference between these crude models is the calculation of the

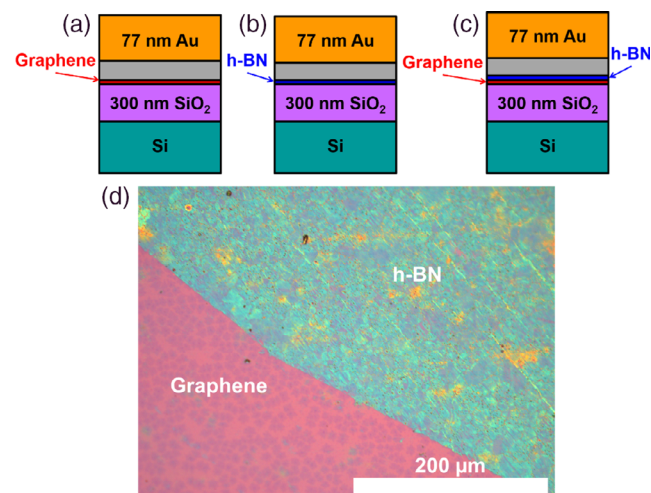


Figure 1. The samples used in this study are CVD-grown a) graphene, b) h-BN, and c) h-BN/G. Samples were coated with a Au thermal transducer (3 nm Ti adhesion layer) for TDTR measurements. The interfaces are considered as Ti/G/SiO₂ or Ti/h-BN/SiO₂ in accordance with studies by Schmidt et al.^[42] where a 5 nm Ti adhesion layer nearly doubled the TBC at the Al–graphite interface. d) An optical microscope image ($\times 20$) showing a $\approx 0.5 \times 0.5 \text{ mm}^2$ area on the surface of h-BN/G sample.

transmission at the interface. The AMM assumes specular reflection at the interface, which is valid only at small temperatures ($T < 30$ K) when the long-wavelength phonons dominate heat transfer.^[54] The aims of MTL and RL are to set upper limits to the phonon transmission and, thus, the TBC. The MTL allows perfect transmission from one side of the interface^[59] and is only limited by the need to satisfy the laws of thermodynamics. In a similar way, the RL assumes that phonons from one side of the interface have a transmission of 1.^[61]

The original derivation of the DMM presented by Swartz and Pohl^[54] assumed diffuse, elastic scattering of phonons at the interface of two materials. A later study by Stoner and Maris^[64] showed that the elastic assumption under-predicts the TBC compared with experimental measurements. More recent work has considered phonon dispersion,^[55] interfacial mixing,^[56] surface roughness,^[57] and inelastic scattering^[58] with varying amounts of success. Nevertheless, the DMM remains a useful tool for capturing trends in phonon transmission across interfaces and because of its simple implementation. An isotropic phonon dispersion is generally assumed, but this assumption is not acceptable in the highly anisotropic, 2D graphene and h-BN. Duda et al.^[65] accounted for this anisotropy and calculated TBC at a metal/graphite interface using an effective 2D Debye density of states (DOS), $D_{2D,eff}(\omega) = \omega / (2\pi v^2 d)$, where ω is angular frequency, v is the phonon group velocity, and d is the interlayer spacing for graphite.

More recently, Chen et al.^[60] showed that this 2D DMM model greatly over-predicts the TBC and presented a new DMM model

using an anisotropic Debye dispersion ($\omega^2 = v_{ab}^2 k_{ab}^2 + v_c^2 k_c^2$, where $k_{ab}^2 = k_a^2 + k_b^2$) referred to here as anisotropic-DMM (A-DMM), where the subscripts pertain to graphite *ab*- (i.e., basal) and *c*-axis. The metal/graphite TBC results by Chen et al.^[60] showed the model still over-predicts the TBC at metal/graphite interfaces when compared with experiments.^[42] An update to the A-DMM reported by Li et al.^[66] attempts to resolve any discrepancy caused by input parameters and uses a piecewise (PW) linear approximation for the flexural (ZA) branch. Herein, this model is referred to as the piecewise anisotropic-DMM (PWA-DMM). More details on the DMM models as well as input parameters are given in the Supporting Information. We implemented both anisotropic DMM models here to calculate the TBC at Ti/G, Ti/ h-BN, and h-BN/G interfaces.

3. Results and Discussion

The optical microscope image in Figure 1d shows a 1×1 mm² area of SiO₂ coated with mostly SLG and h-BN. Figure 2a-b shows the Raman spectra from the sample used in this study. The graphene sample (Figure 2a) with G peak at 1592 cm⁻¹ (E_{2g} mode near the Γ point) and 2D peak at 2703 cm⁻¹ (A_{1g} mode near the K point)^[67] and intensity ratio $I(2D)/I(G) \approx 2.2$ ^[68] shows our sample is single layer; however, the shift in peak positions and reduced $I(2D)/I(G)$ ratio suggests some p-type doping^[69,70]

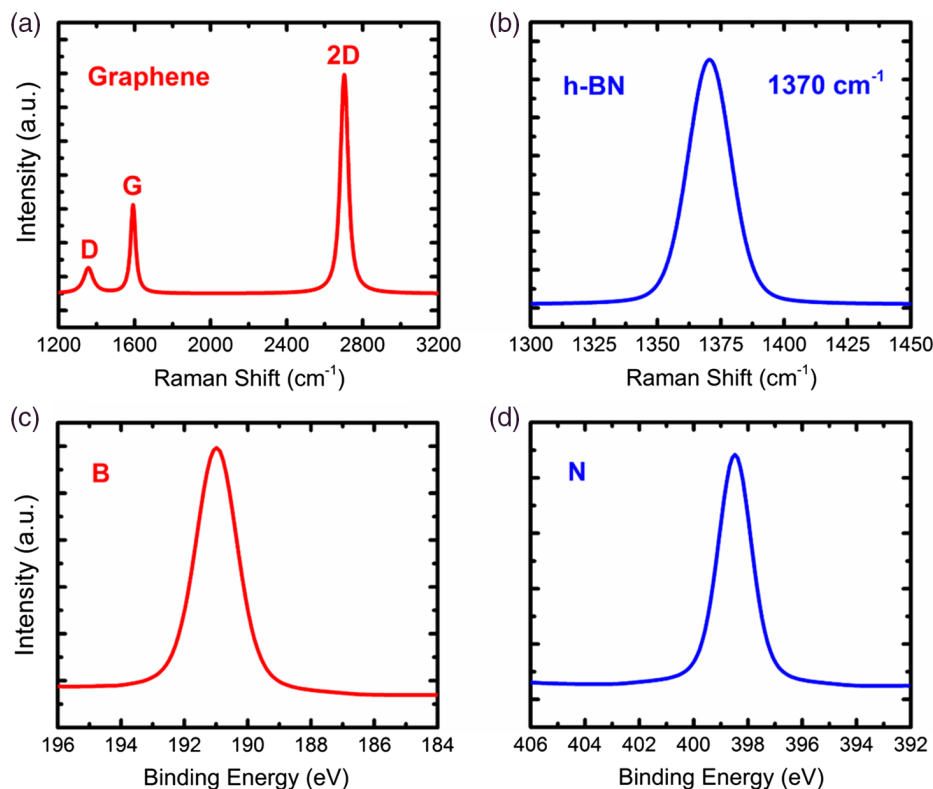


Figure 2. a) Graphene and b) h-BN Raman spectra. The intensity ratio $I(2D)/I(G) \approx 2.2$ ^[68] in (a) indicates graphene sample is single layer. High-resolution XPS spectra for h-BN samples showing c) B and d) N peaks at 191 and 398 eV, respectively. From the XPS data, we determined that the stoichiometry of our h-BN sample was 1.17:1 (B:N).^[80]

previously attributed to residual PMMA.^[71] The D peak at 1356 cm^{-1} arises from disorder in the graphene layer. Figure 2b shows that the peak in h-BN Raman spectrum blue shifted to $\approx 1370\text{ cm}^{-1}$, corresponding to the in-plane E_{2g} mode, compared with the characteristic peak at $\approx 1366\text{ cm}^{-1}$ for bulk h-BN.^[72] This shift could be caused by stress in the film resulting from the growth process, substrate/interlayer interaction, or crystallite size.^[73–75] A comparison of the graphene and h-BN/graphene Raman spectra (not shown) did not display new peaks in the range of $1200\text{--}3200\text{ cm}^{-1}$ which would suggest coupling between the 2D layers.^[76–79] There was simply peak broadening around 1360 cm^{-1} as a result of the h-BN layer. A more extensive Raman study may reveal shear or layer-breathing modes at lower frequencies. The high-resolution XPS spectra in Figure 2c,d, respectively, show B and N peaks at binding energies of 191 and 398 eV, respectively. From the XPS data, the stoichiometry of our h-BN sample was 1.17:1 (B:N).^[80]

The TBC at Ti/G/SiO₂ and Ti/h-BN/SiO₂ interfaces was $30.6 (+6.2/-4.2)$ and $33.7 (+9.8/-5.3)\text{ MW m}^{-2}\text{ K}^{-1}$, respectively. The TBC at Ti/h-BN/G/SiO₂ interface was $18.3 (+4.0/-2.7)\text{ MW m}^{-2}\text{ K}^{-1}$. The TDTR signals for these samples are shown in Figure 3a. The total interfacial thermal conductance

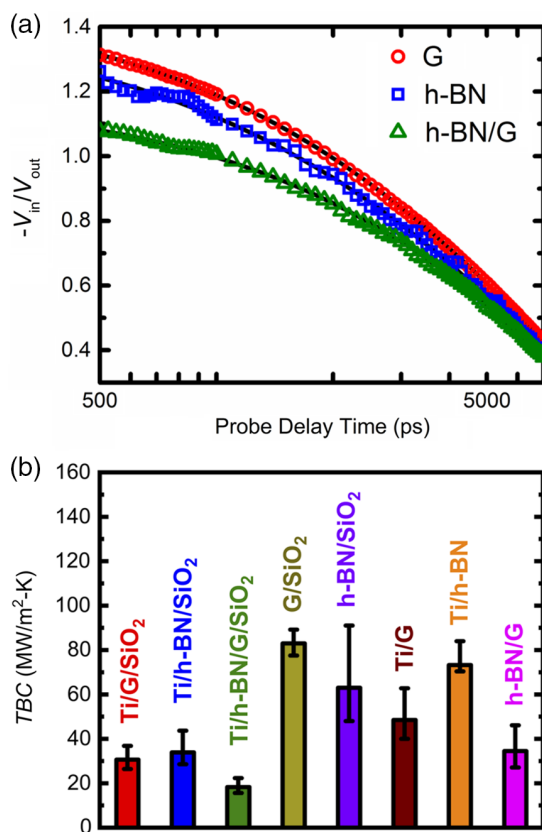


Figure 3. a) TDTR signal comparisons for three samples used in this study. b) Summary of TBC results from TDTR measurements and thermal resistor network. Ti/G/SiO₂, Ti/h-BN/SiO₂, and Ti/h-BN/G/SiO₂ values measured using TDTR. Error bars were calculated using an MC method.^[49] G/SiO₂ and h-BN/SiO₂ data taken from previous studies,^[88,89] respectively. Ti/G, Ti/h-BN, and h-BN/G TBC values estimated using series resistance approximation.

per unit area can be ascribed to the metal/h-BN/G/SiO₂ interfaces acting in series, as in the case of a thin-film sample between two solids.^[81] We, therefore, use a 1D thermal resistance network to estimate the TBC at h-BN/G interface. This method was used previously^[82–86] where the heat transport across metal/G/SiO₂ and metal/G/metal interfaces was treated as the resistance of the decoupled metal/G and G/SiO₂ (or G/metal) interfaces acting in series. Zheng et al.^[86] reevaluated this analysis recently, suggesting that long-wavelength phonons may traverse both interfaces through a process similar to the heat transport in superlattices.^[87] Nevertheless, we apply the method here in the following manner. Using the relationship $1/\text{TBC}_{\text{Ti/G/SiO}_2} = 1/\text{TBC}_{\text{Ti/G}} + 1/\text{TBC}_{\text{G/SiO}_2}$, we can determine $\text{TBC}_{\text{Ti/G}}$. Similarly, the $\text{TBC}_{\text{G/SiO}_2}$ term in this equation can be replaced by $\text{TBC}_{\text{h-BN/SiO}_2}$ to determine $\text{TBC}_{\text{Ti/h-BN}}$. The thermal conductance of the h-BN and SLG layers was much greater than the interfacial TBC and was therefore neglected.

The $\text{TBC}_{\text{G/SiO}_2}$ and $\text{TBC}_{\text{h-BN/SiO}_2}$ values were previously reported for SLG [$\approx 83 (+6.2/-5.5)\text{ MW m}^{-2}\text{ K}^{-1}$]^[88] and monolayer h-BN [$\approx 63 (+28/-15)\text{ MW m}^{-2}\text{ K}^{-1}$]^[89] using the 3ω technique. Using these values, the resulting $\text{TBC}_{\text{Ti/G}}$ and $\text{TBC}_{\text{Ti/h-BN}}$ are $48.5 (+8.5/-14.3)$ and $73.3 (+10.7/-2.9)\text{ MW m}^{-2}\text{ K}^{-1}$, respectively. The uncertainty bounds were determined using the upper/lower limits from the MC simulations for Ti/G/SiO₂ and Ti/h-BN/SiO₂ interfaces. We use these values and formulate a new relationship, $1/\text{TBC}_{\text{Ti/h-BN/G/SiO}_2} = 1/\text{TBC}_{\text{Ti/h-BN}} + 1/\text{TBC}_{\text{h-BN/G}} + 1/\text{TBC}_{\text{G/SiO}_2}$, and estimate $\text{TBC}_{\text{h-BN/G}}$ to be $34.5 (+11.6/-7.4)\text{ MW m}^{-2}\text{ K}^{-1}$. The TBC values are summarized in Figure 3b. When compared with previous values in literature, our TBC value is greater than $7.4\text{ MW m}^{-2}\text{ K}^{-1}$ reported by Chen et al.^[35] and $5\text{--}10\text{ MW m}^{-2}\text{ K}^{-1}$ reported by Kim et al.^[38] However, our value is less than $52.2\text{ MW m}^{-2}\text{ K}^{-1}$ reported by Liu et al.,^[37] which we attribute to surface roughness resulting from the CVD growth process and PMMA residue following the transfer process. Our value is also in the similar range as TBC ($30\text{--}50\text{ MW m}^{-2}\text{ K}^{-1}$) for different lattice stacking configurations predicted using first-principles AGF simulations.^[31]

The DMM does not consider the quality of the interface (e.g., bonding, roughness), which varies from sample to sample; therefore, we hold α_{12} constant and determined its value for each interface by fitting both DMM models to our RT TDTR measurements (Table 1). As a result, only the phonon irradiation from material 1 (e.g., Ti in the case of Ti/G and Ti/h-BN interface) needs to be considered.^[54] Thus, when utilizing the fitted values, $\alpha_{12,\text{fit}}$, the A-DMM and PWA-DMM models differ from each other, and from the original DMM (Equation S2, Supporting Information), only when considering the h-BN/G interface. The $\alpha_{12,\text{fit}}$ values shown in Table 1 are very insightful. As expected, $\alpha_{12,\text{fit}}$ for the Ti/G and Ti/h-BN is identical for the A-DMM and PWA-DMM models. They are also similar order

Table 1. Fitted phonon transmission coefficients, $\alpha_{12,\text{fit}}$, used in DMM analysis determined by fitting to RT TDTR data.

Interface	A-DMM ^[45]	PWA-DMM ^[46]
Ti/G	0.05424	0.05424
Ti/h-BN	0.08016	0.08016
h-BN/G	0.02494	0.2287

of magnitude ($\approx 10^{-2}$) as $\alpha_{12,fit}$ at metal/graphite interfaces^[42,82] reported in previous studies. We must point out that Schmidt et al.^[42] assumed a sine-type (or Born-von Karman)^[59] dispersion for metals and effective 2D Debye DOS^[65] in graphite. Also, the velocities of each phonon polarization were lumped into a single, average velocity. Koh et al.^[82] used a linear (Debye) dispersion for Au. $\alpha_{12,fit}$ for h-BN/G interface predicted by the PWA-DMM was nearly an order of magnitude larger than the value predicted by the A-DMM (see Table 1). The reason for this discrepancy is discussed in the following paragraphs.

The ratio of α_{12} , calculated using phonon irradiation (Equation S3 and S4, Supporting Information) and the relationship $\alpha_{12} = H_2/(H_1 + H_2)$, to $\alpha_{12,fit}$ values in Table 1 is shown in **Figure 4a**. While Li et al.^[66] made an elastic assumption in determining $\alpha_{12}(\omega)$, we assume inelastic scattering^[90] in accordance with the A-DMM model when computing $\alpha_{12}(T)$, allowing phonons of all frequencies in h-BN and graphene to participate. For the h-BN/G interface, α_{12} is expected to be close to 0.5 for both models due to the similar vibrational properties of graphene

and h-BN.^[91,92] The graph of $\alpha_{12}/\alpha_{12,fit}$ in Figure 4a shows a weak temperature dependence above 200 K for both the A-DMM model (solid lines) and PWA-DMM (dashed lines). The discrepancy between α_{12} and $\alpha_{12,fit}$ was much larger for A-DMM compared with the PWA-DMM model. RT $\alpha_{12}/\alpha_{12,fit}$ for Ti/G and Ti/h-BN interfaces are 14.9 and 7.27, respectively, using the A-DMM model, whereas there is much better agreement for the PWA-DMM (1.36 and 1.55 for Ti/G and Ti-h-BN, respectively).

The high $\alpha_{12}/\alpha_{12,fit}$ ratio for the A-DMM for Ti/G and Ti/h-BN interfaces arises from the much higher phonon irradiation in graphene and h-BN compared with the PWA-DMM. The phonon irradiation is proportional to v_{ab}^{-2} ; thus, the assumption of a constant v_{ab} for TL2 branch, which contributes most to the irradiation,^[60,66] results in a much higher calculated α_{12} value for A-DMM model. This is the phonon-focusing^[93] effect whereby cross-plane TBC can be increased with a reduction in in-plane phonon velocity. The same is true for h-BN/G interface where $\alpha_{12}/\alpha_{12,fit}$ was 30.3 and 1.57 for the A-DMM and PWA-DMM models, respectively. The transmission coefficient for each phonon branch, $\alpha_{12,j}$, is shown in Figure 4b and further reinforces the importance of the TL2 branch.

Finally, the TBC predicted using $\alpha_{12,fit}$ is shown in **Figure 5** along with TBC for Ti/G, Ti/h-BN, and h-BN/G from our TDTR results. Various literature results for h-BN/G,^[35,37,38] metal/G,^[83,86,94] and metal/graphite^[42] interfaces are also shown for comparison. The discrepancy between h-BN/G results for the A-DMM and PWA-DMM models at low temperatures arises from the assumption of constant α_{12} . The phonon characteristic wavelength varies as T^{-1} , resulting in higher α_{12} at low temperatures where the phonon characteristic wavelength is much

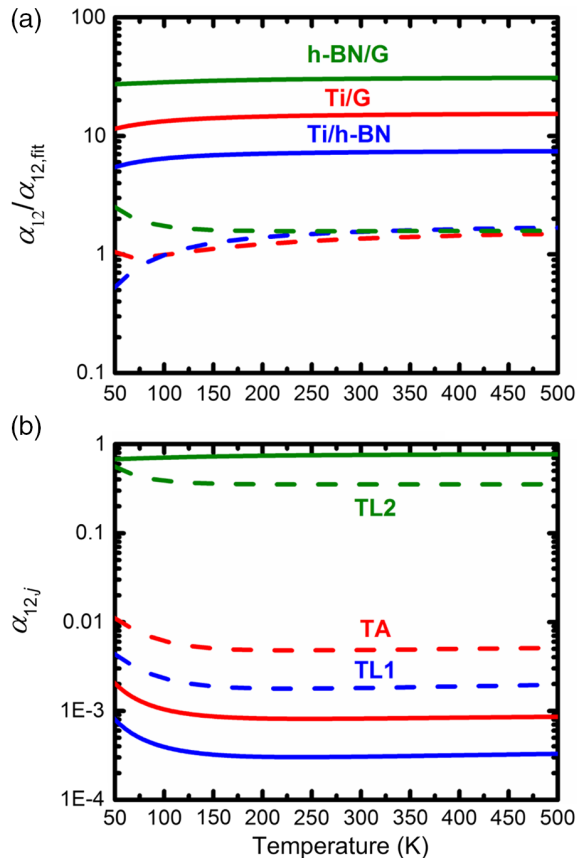


Figure 4. a) Ratio of transmission coefficients, $\alpha_{12}/\alpha_{12,fit}$, for A-DMM (solid lines) and PWA-DMM (dashed lines), where α_{12} is calculated from phonon irradiation (Equation S3 and S4, Supporting Information) and the relationship $\alpha_{12} = H_2/(H_1 + H_2)$ and $\alpha_{12,fit}$ is determined from RT TDTR data. The ratio $\alpha_{12}/\alpha_{12,fit}$ depends weakly on temperature above 200 K. b) The transmission coefficients, $\alpha_{12,j}$, of different phonon branches (TA, TL1, TL2) as a function of temperature highlight the importance of the TL2 branch to the total transmission α_{12} for h-BN/G interface. Here, solid lines are for A-DMM and dashed lines for PWA-DMM.

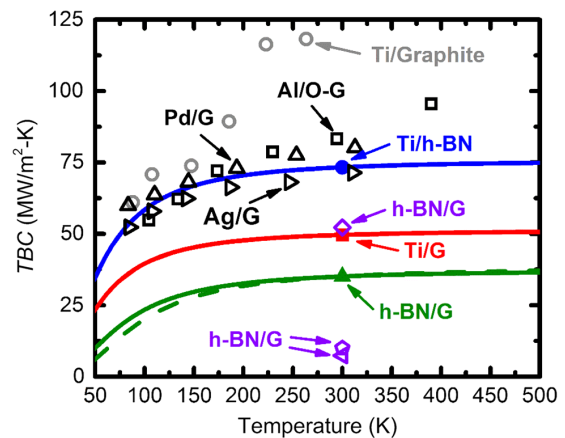


Figure 5. Comparison of TBC for Ti/G (filled red square), Ti/h-BN (filled blue circle), and h-BN/G (filled green triangle) interfaces from this work. DMM results from this work are plotted as solid (A-DMM) and dashed lines (PWA-DMM). TBC values at Ti/G, Ti/h-BN, and h-BN/G interfaces are estimated assuming series resistances. The DMM results were calculated using $\alpha_{12,fit}$ values in Table 1. Also shown are previously reported values of h-BN/G TBC from studies by Chen et al.^[35] (open left purple triangle), Liu et al.^[37] (open purple diamond), and Kim et al.^[38] (open purple trapezoid) using Raman spectroscopy. For further comparison, TBC for various metal/G [Al/O-G (open black square),^[83] Pd/G (open up black triangle),^[94] and Ag/G (open right black triangle)^[86] and Ti/graphite (open grey circles)^[42] interfaces are also shown.

larger than surface roughness, leading to decreased scattering.^[54] This behavior is captured by the PWA-DMM model but not A-DMM. Interestingly, the TBC at h-BN/G interface is constant above 200 K for both models. TBC is expected to increase below the Debye temperature,^[54,95] which is greater than 1000 K^[96] for both h-BN and graphene.

The observed trend with temperature may be a result of the ZA branch in *ab*-axis and LA branch in *c*-axis (i.e., TL2 branch), being the dominant contributor to TBC for both A-DMM and PWA-DMM models. The maximum frequency of vibrations (Table S1, Supporting Information) for the two branches corresponds to Debye temperatures of 764 and 174 K, respectively, but the contribution from both remains constant above 200 K. Zhang et al.^[36] used MD simulations to show increased TBC from 200 to 700 K which the authors attributed to contributions from high-frequency phonons at elevated temperatures. Our implementation of the DMM only includes the contributions of acoustic phonons which are the dominant heat carriers in the h-BN/G material system^[31,36] due to the large DOS for ZA phonons at low frequencies.^[51,82,97–99] Frequency-dependent phonon transmission and TBC reported by Yan et al.^[31] have revealed this fact in vertically stacked h-BN/G/h-BN interfaces with the large DOS mismatch resulting in smaller transmission at high frequencies. In-plane modes have larger contribution for smaller interfacial separation distance. Inelastic phonon processes which occur at elevated temperatures^[100] may not be accurately captured by the DMM model. The low-frequency out-of-plane modes are major contributors to the thermal conductivity of superlattices composed of in-plane h-BN/G heterostructures as well and are greatly influenced by the period and overall length.^[101–106]

4. Conclusion

We have estimated the TBC at h-BN/G interface using a series thermal resistor network coupled with TDTR measurements at Ti/G/SiO₂, Ti/h-BN/SiO₂, and Ti/h-BN/G/SiO₂ interfaces. As h-BN and graphene have similar physical structures and acoustic properties, the h-BN/G TBC may be increased by improving sample quality. We compare phonon transmission using two forms of the DMM for anisotropic materials. The A-DMM model predicts a higher phonon irradiation, thus higher transmission coefficient due to the assumption of constant velocity of the ZA mode across the entire first Brillouin zone (FBZ). The PWA-DMM model uses two different phonon velocities, near the center and at edge of the FBZ, resulting in better prediction of phonon transmission. The phonon transmission and temperature dependence of TBC confirm the ZA branch along the *ab*-axis, and the LA branch along the *c*-axis of graphene and h-BN are the dominant contributors when implementing both the A-DMM and PWA-DMM model. This methodology can be extended to other 2D heterostructures to analyze the TBC at the interfaces of 2D layers.

Supporting Information

Supporting Information is available from the Wiley Online Library or from the author.

Acknowledgements

D.B.B. was supported by a National Science Foundation Graduate Research Fellowship under grant no. DGE-1650044. Any opinion, findings, and conclusions or recommendations expressed in this material are those of the authors and do not necessarily reflect the views of the National Science Foundation.

Conflict of Interest

The authors declare no conflict of interest.

Keywords

graphene, hexagonal boron nitride, phonon transmissions, thermal boundary conductance

Received: June 5, 2019

Revised: September 13, 2019

Published online: November 12, 2019

- [1] K. S. Novoselov, D. Jiang, F. Schedin, T. J. Booth, V. V. Khotkevich, S. V. Morozov, A. K. Geim, *Proc. Natl. Acad. Sci. USA* **2005**, *102*, 10451.
- [2] K. S. Novoselov, A. K. Geim, S. V. Morozov, D. Jiang, Y. Zhang, S. V. Dubonos, I. V. Grigorieva, A. A. Firsov, *Science* **2004**, *306*, 666.
- [3] A. A. Balandin, S. Ghosh, W. Bao, I. Calizo, D. Teweldebrhan, F. Miao, C. N. Lau, *Nano Lett.* **2008**, *8*, 902.
- [4] K. I. Bolotin, K. J. Sikes, Z. Jiang, M. Klima, G. Fudenberg, J. Hone, P. Kim, H. L. Stormer, *Solid State Commun.* **2008**, *146*, 351.
- [5] C. Lee, X. D. Wei, J. W. Kysar, J. Hone, *Science* **2008**, *321*, 385.
- [6] R. R. Nair, P. Blake, A. N. Grigorenko, K. S. Novoselov, T. J. Booth, T. Stauber, N. M. Peres, A. K. Geim, *Science* **2008**, *320*, 1308.
- [7] C. R. Dean, A. F. Young, I. Meric, C. Lee, L. Wang, S. Sorgenfrei, K. Watanabe, T. Taniguchi, P. Kim, K. L. Shepard, J. Hone, *Nat. Nanotechnol.* **2010**, *5*, 722.
- [8] A. S. Mayorov, R. V. Gorbachev, S. V. Morozov, L. Britnell, R. Jalil, L. A. Ponomarenko, P. Blake, K. S. Novoselov, K. Watanabe, T. Taniguchi, A. K. Geim, *Nano Lett.* **2011**, *11*, 2396.
- [9] L. Britnell, R. V. Gorbachev, R. Jalil, B. D. Belle, F. Schedin, A. Mishchenko, T. Georgiou, M. I. Katsnelson, L. Eaves, S. V. Morozov, N. M. R. Peres, *Science* **2012**, *335*, 947.
- [10] K. H. Lee, H. J. Shin, J. Lee, I. Y. Lee, G. H. Kim, J. Y. Choi, S. W. Kim, *Nano Lett.* **2012**, *12*, 714.
- [11] L. Britnell, R. M. Ribeiro, A. Eckmann, R. Jalil, B. D. Belle, A. Mishchenko, Y. J. Kim, R. V. Gorbachev, T. Georgiou, S. V. Morozov, A. N. Grigorenko, *Science* **2013**, *340*, 1311.
- [12] T. Georgiou, R. Jalil, B. D. Belle, L. Britnell, R. V. Gorbachev, S. V. Morozov, Y. J. Kim, A. Gholinia, S. J. Haigh, O. Makarovskiy, L. Eaves, *Nat. Nanotechnol.* **2013**, *8*, 100.
- [13] W. J. Yu, Z. Li, H. Zhou, Y. Chen, Y. Wang, Y. Huang, X. Duan, *Nat. Mater.* **2013**, *12*, 246.
- [14] A. K. Geim, I. V. Grigorieva, *Nature* **2013**, *499*, 419.
- [15] K. S. Novoselov, A. Mishchenko, A. Carvalho, A. H. C. Neto, *Science* **2016**, *353*, aac9439.
- [16] Y. Liu, N. O. Weiss, X. D. Duan, H. C. Cheng, Y. Huang, X. F. Duan, *Nat. Rev. Mater.* **2016**, *1*, 16042.
- [17] C. C. Chen, Z. Li, L. Shi, S. B. Cronin, *Nano Res.* **2015**, *8*, 666.
- [18] R. D'Souza, S. Mukherjee, *Phys. E* **2016**, *81*, 96.
- [19] Y. Ding, Y. Wang, J. Ni, *Appl. Phys. Lett.* **2009**, *95*, 123105.

- [20] L. Ci, L. Song, C. Jin, D. Jariwala, D. Wu, Y. Li, A. Srivastava, Z. F. Wang, K. Storr, L. Balicas, F. Liu, *Nat. Mater.* **2010**, *9*, 430.
- [21] G. Seol, J. Guo, *Appl. Phys. Lett.* **2011**, *98*, 143107.
- [22] K. Yang, Y. Chen, R. D'Agosta, Y. Xie, J. Zhong, A. Rubio, *Phys. Rev. B* **2012**, *86*, 045425.
- [23] Y. Gao, Y. Zhang, P. Chen, Y. Li, M. Liu, T. Gao, D. Ma, Y. Chen, Z. Cheng, X. Qiu, W. Duan, *Nano Lett.* **2013**, *13*, 3439.
- [24] Z. Liu, L. Ma, G. Shi, W. Zhou, Y. Gong, S. Lei, X. Yang, J. Zhang, J. Yu, K. P. Hackenberg, A. Babakhani, *Nat. Nanotechnol.* **2013**, *8*, 119.
- [25] Y. Yokomizo, J. Nakamura, *Appl. Phys. Lett.* **2013**, *103*, 113901.
- [26] G. Giovannetti, P. A. Khomyakov, G. Brocks, P. J. Kelly, J. van den Brink, *Phys. Rev. B* **2007**, *76*, 073103.
- [27] R. Decker, Y. Wang, V. W. Brar, W. Regan, H. Z. Tsai, Q. Wu, W. Gannett, A. Zettl, M. F. Crommie, *Nano Lett.* **2011**, *11*, 2291.
- [28] B. Sachs, T. O. Wehling, M. I. Katsnelson, A. I. Lichtenstein, *Phys. Rev. B* **2011**, *84*, 195414.
- [29] J. M. Xue, J. Sanchez-Yamagishi, D. Bulmash, P. Jacquod, A. Deshpande, K. Watanabe, T. Taniguchi, P. Jarillo-Herrero, B. J. LeRoy, *Nat. Mater.* **2011**, *10*, 282.
- [30] G. J. Slotman, G. A. de Wijs, A. Fasolino, M. I. Katsnelson, *Ann. Phys.* **2014**, *526*, 381.
- [31] Z. Q. Yan, L. Chen, M. N. Yoon, S. Kumar, *Nanoscale* **2016**, *8*, 4037.
- [32] E. Pop, *Nano Res.* **2010**, *3*, 147.
- [33] P. L. Kapitza, *J. Phys. USSR* **1941**, *5*, 59.
- [34] R. Mao, B. D. Kong, K. W. Kim, T. Jayasekera, A. Calzolari, M. B. Nardelli, *Appl. Phys. Lett.* **2012**, *101*, 113111.
- [35] C. C. Chen, Z. Li, L. Shi, S. B. Cronin, *Appl. Phys. Lett.* **2014**, *104*, 081908.
- [36] J. C. Zhang, Y. Hong, Y. A. Yue, *J. Appl. Phys.* **2015**, *117*, 134307.
- [37] Y. Liu, Z. Y. Ong, J. Wu, Y. Zhao, K. Watanabe, T. Taniguchi, D. Chi, G. Zhang, J. T. Thong, C. W. Qiu, K. Hippalgaonkar, *Sci. Rep.* **2017**, *7*, 43886.
- [38] D. Kim, H. Kim, W. S. Yun, K. Watanabe, T. Taniguchi, H. Rho, M. H. Bae, *2D Mater.* **2018**, *5*, 025009.
- [39] Z. Liu, L. Song, S. Zhao, J. Huang, L. Ma, J. Zhang, J. Lou, P. M. Ajayan, *Nano Lett.* **2011**, *11*, 2032.
- [40] Y. C. Lin, C. C. Lu, C. H. Yeh, C. H. Jin, K. Suenaga, P. W. Chiu, *Nano Lett.* **2012**, *12*, 414.
- [41] B. Huang, Y. K. Koh, *Carbon* **2016**, *105*, 268.
- [42] A. J. Schmidt, K. C. Collins, A. J. Minnich, G. Chen, *J. Appl. Phys.* **2010**, *107*, 104907.
- [43] R. M. Costescu, M. A. Wall, D. G. Cahill, *Phys. Rev. B* **2003**, *67*, 054302.
- [44] D. G. Cahill, *Rev. Sci. Instrum.* **2004**, *75*, 5119.
- [45] Y. K. Koh, D. G. Cahill, *Phys. Rev. B* **2007**, *76*, 075207.
- [46] A. J. Schmidt, X. Y. Chen, G. Chen, *Rev. Sci. Instrum.* **2008**, *79*, 114902.
- [47] P. E. Hopkins, C. M. Reinke, M. F. Su, R. H. Olsson, E. A. Shaner, Z. C. Leseman, J. R. Serrano, L. M. Phinney, I. El-Kady, *Nano Lett.* **2011**, *11*, 107.
- [48] J. Liu, J. Zhu, M. Tian, X. K. Gu, A. Schmidt, R. G. Yang, *Rev. Sci. Instrum.* **2013**, *84*, 034902.
- [49] T. L. Bougher, L. Yates, C. F. Lo, W. Johnson, S. Graham, B. A. Cola, *Nanoscale Microscale Thermophys. Eng.* **2016**, *20*, 22.
- [50] D. B. Brown, T. L. Bougher, B. A. Cola, S. Kumar, *Carbon* **2018**, *139*, 913.
- [51] R. Prasher, *Appl. Phys. Lett.* **2009**, *94*, 041905.
- [52] R. S. Prasher, P. E. Phelan, *J. Heat Transfer* **2001**, *123*, 105.
- [53] W. A. Little, *Can. J. Phys.* **1959**, *37*, 334.
- [54] E. T. Swartz, R. O. Pohl, *Rev. Mod. Phys.* **1989**, *61*, 605.
- [55] P. Reddy, K. Castelino, A. Majumdar, *Appl. Phys. Lett.* **2005**, *87*, 211908.
- [56] T. Beechem, S. Graham, P. Hopkins, P. Norris, *Appl. Phys. Lett.* **2007**, *90*, 054104.
- [57] P. E. Hopkins, L. M. Phinney, J. R. Serrano, T. E. Beechem, *Phys. Rev. B* **2010**, *82*, 085307.
- [58] P. E. Hopkins, J. C. Duda, P. M. Norris, *J. Heat Transfer* **2011**, *133*, 062401.
- [59] C. Dames, G. Chen, *J. Appl. Phys.* **2004**, *95*, 682.
- [60] Z. Chen, Z. Wei, Y. Chen, C. Dames, *Phys. Rev. B* **2013**, *87*, 125426.
- [61] N. S. Snyder, *Cryogenics* **1970**, *10*, 89.
- [62] H. K. Lyeo, D. G. Cahill, *Phys. Rev. B* **2006**, *73*, 144301.
- [63] C. Monachon, G. Schusteritsch, E. Kaxiras, L. Weber, *J. Appl. Phys.* **2014**, *115*, 123509.
- [64] R. J. Stoner, H. J. Maris, *Phys. Rev. B* **1993**, *48*, 16373.
- [65] J. C. Duda, J. L. Smoyer, P. M. Norris, P. E. Hopkins, *Appl. Phys. Lett.* **2009**, *95*, 031912.
- [66] H. K. Li, W. D. Zheng, Y. K. Koh, *Phys. Rev. Mater.* **2018**, *2*, 123802.
- [67] R. J. Nemanich, S. A. Solin, *Phys. Rev. B* **1979**, *20*, 392.
- [68] A. C. Ferrari, J. C. Meyer, V. Scardaci, C. Casiraghi, M. Lazzeri, F. Mauri, S. Piscanec, D. Jiang, K. S. Novoselov, S. Roth, A. K. Geim, *Phys. Rev. Lett.* **2006**, *97*, 187401.
- [69] J. Yan, Y. B. Zhang, P. Kim, A. Pinczuk, *Phys. Rev. Lett.* **2007**, *98*, 166802.
- [70] A. Das, S. Pisana, B. Chakraborty, S. Piscanec, S. K. Saha, U. V. Waghmare, K. S. Novoselov, H. R. Krishnamurthy, A. K. Geim, A. C. Ferrari, A. K. Sood, *Nat. Nanotechnol.* **2008**, *3*, 210.
- [71] A. Pirkle, J. Chan, A. Venugopal, D. Hinojos, C. W. Magnuson, S. McDonnell, L. Colombo, E. M. Vogel, R. S. Ruoff, R. M. Wallace, *Appl. Phys. Lett.* **2011**, *99*, 122108.
- [72] R. Geick, C. H. Perry, G. Rupprecht, *Phys. Rev.* **1966**, *146*, 543.
- [73] R. J. Nemanich, S. A. Solin, R. M. Martin, *Phys. Rev. B* **1981**, *23*, 6348.
- [74] R. Arenal, A. C. Ferrari, S. Reich, L. Wirtz, J. Y. Mevellec, S. Lefrant, A. Rubio, A. Loiseau, *Nano Lett.* **2006**, *6*, 1812.
- [75] L. Song, L. Ci, H. Lu, P. B. Sorokin, C. Jin, J. Ni, A. G. Kvashnin, D. G. Kvashnin, J. Lou, B. I. Yakobson, P. M. Ajayan, *Nano Lett.* **2010**, *10*, 3209.
- [76] M. H. Chiu, M. Y. Li, W. Zhang, W. T. Hsu, W. H. Chang, M. Terrones, H. Terrones, L. J. Li, *ACS Nano* **2014**, *8*, 9649.
- [77] C. H. Lui, Z. Ye, C. Ji, K. C. Chiu, C. T. Chou, T. I. Andersen, C. Means-Shively, H. Anderson, J. M. Wu, T. Kidd, Y. H. Lee, *Phys. Rev. B* **2015**, *91*, 165403.
- [78] K. Wang, B. Huang, M. Tian, F. Ceballos, M. W. Lin, M. Mahjour-Samani, A. Boulesbaa, A. A. Puzos, C. M. Rouleau, M. Yoon, H. Zhao, *ACS Nano* **2016**, *10*, 6612.
- [79] C. Jin, J. Kim, J. Suh, Z. Shi, B. Chen, X. Fan, M. Kam, K. Watanabe, T. Taniguchi, S. Tongay, A. Zettl, *Nat. Phys.* **2017**, *13*, 127.
- [80] G. C. Smith, *Surface Analysis by Electron Spectroscopy: Measurement and Interpretation*, Updates in applied physics and electrical technology, Plenum Press, New York, NY **1994**, p. xi, 156 p.
- [81] S. M. Lee, D. G. Cahill, *Microscale Thermophys. Eng.* **1997**, *1*, 47.
- [82] Y. K. Koh, M. H. Bae, D. G. Cahill, E. Pop, *Nano Lett.* **2010**, *10*, 4363.
- [83] P. E. Hopkins, M. Baraket, E. V. Barnat, T. E. Beechem, S. P. Kearney, J. C. Duda, J. T. Robinson, S. G. Walton, *Nano Lett.* **2012**, *12*, 590.
- [84] J. Yang, E. Ziade, C. Maragliano, R. Crowder, X. Wang, M. Stefancich, M. Chiesa, A. K. Swan, A. J. Schmidt, *J. Appl. Phys.* **2014**, *116*, 023515.
- [85] B. M. Foley, S. C. Hernandez, J. C. Duda, J. T. Robinson, S. G. Walton, P. E. Hopkins, *Nano Lett.* **2015**, *15*, 4876.
- [86] W. D. Zheng, B. Huang, H. K. Li, Y. K. Koh, *ACS Appl. Mater. Interfaces* **2018**, *10*, 35487.
- [87] Y. K. Koh, Y. Cao, D. G. Cahill, D. Jena, *Adv. Funct. Mater.* **2009**, *19*, 610.
- [88] Z. Chen, W. Jang, W. Bao, C. N. Lau, C. Dames, *Appl. Phys. Lett.* **2009**, *95*, 161910.
- [89] X. Li, Y. Yan, L. Dong, J. Guo, A. Aiyiti, X. Xu, B. Li, *J. Phys. D Appl. Phys.* **2017**, *50*, 104002.
- [90] G. Chen, *Phys. Rev. B* **1998**, *57*, 14958.

- [91] L. Wirtz, A. Rubio, *Solid State Commun.* **2004**, *131*, 141.
- [92] J. Serrano, A. Bosak, R. Arenal, M. Krisch, K. Watanabe, T. Taniguchi, H. Kanda, A. Rubio, L. Wirtz, *Phys. Rev. Lett.* **2007**, *98*, 095503.
- [93] J. P. Wolfe, *Imaging Phonons: Acoustic Wave Propagation in Solids*, Cambridge University Press, Cambridge, UK; New York, NY **1998**, p. xiii, 411 p.
- [94] B. Huang, Y. K. Koh, *Adv. Mater. Interfaces* **2017**, *4*, 1700559.
- [95] G. Chen, *Nanoscale Energy Transport and Conversion: A Parallel Treatment of Electrons, Molecules, Phonons, and Photons*, MIT-Pappalardo series in mechanical engineering, Oxford University Press, New York, NY **2005**, p. xxiii, 531 p.
- [96] T. Tohei, A. Kuwabara, F. Oba, I. Tanaka, *Phys. Rev. B* **2006**, *73*, 064304.
- [97] L. Lindsay, D. A. Broido, N. Mingo, *Phys. Rev. B* **2010**, *82*, 115427.
- [98] J. H. Seol, I. Jo, A. L. Moore, L. Lindsay, Z. H. Aitken, M. T. Pettes, X. Li, Z. Yao, R. Huang, D. Broido, N. Mingo, *Science* **2010**, *328*, 213.
- [99] I. Jo, I. K. Hsu, Y. J. Lee, M. M. Sadeghi, S. Kim, S. Cronin, E. Tutuc, S. K. Banerjee, Z. Yao, L. Shi, *Nano Lett.* **2011**, *11*, 85.
- [100] Z. Y. Ong, E. Pop, *Phys. Rev. B* **2010**, *81*, 155408.
- [101] J.-W. Jiang, J.-S. Wang, B.-S. Wang, *Appl. Phys. Lett.* **2011**, *99*, 043109.
- [102] H. Sevinçli, W. Li, N. Mingo, G. Cuniberti, S. Roche, *Phys. Rev. B* **2011**, *84*, 205444.
- [103] S. Li, Z. Ren, J. Zheng, Y. Zhou, Y. Wan, L. Hao, *J. Appl. Phys.* **2013**, *113*, 033703.
- [104] T. Zhu, E. Ertekin, *Phys. Rev. B* **2014**, *90*, 195209.
- [105] X.-K. Chen, Z.-X. Xie, W.-X. Zhou, L.-M. Tang, K.-Q. Chen, *Appl. Phys. Lett.* **2016**, *109*, 023101.
- [106] X.-K. Chen, Z.-X. Xie, W.-X. Zhou, L.-M. Tang, K.-Q. Chen, *Carbon* **2016**, *100*, 492.